TRANSACTIONS
OF TIANJIN UNIVERSITY

2016, 22: 035-042
DOI 10.1007/s12209-016-2527-z

3D Finite Element Analysis of TBM Water Diversion Tunnel Segment Coupled with Seepage Field*

Zhong Denghua(钟登华), Hu Nengming(胡能明), Cheng Zhengfei(程正飞),
Lü Peng(吕　鹏), Tong Dawei(佟大威)
(State Key Laboratory of Hydraulic Engineering Simulation and Safety, Tianjin University, Tianjin 300072, China)

Abstract: In most studies of tunnel boring machine (TBM) tunnelling, the groundwater pressure was not considered, or was simplified and exerted on the boundary of lining structure. Meanwhile, the leakage, which mainly occurs in the segment joints, was often ignored in the relevant studies of TBM tunnelling. Additionally, the geological models in these studies were simplified to different extents, and mostly were simplified as homogenous bodies. Considering the deficiencies above, a 3D refined model of the surrounding rock of a tunnel is firstly established using NURBS-TIN-BReP hybrid data structure in this paper. Then the seepage field of the surrounding rock considering the leakage in the segment joints is simulated. Finally, the stability of TBM water diversion tunnel is studied coupled with the seepage simulation, to analyze the stress-strain conditions, the axial force and the bending moment of tunnel segment considering the leakage in the segment joints. The results illustrate that the maximum radial displacement, the minimum principal stress, the maximum principal stress and the axial force of segment lining considering the seepage effect are all larger than those disregarding the seepage effect.
Keywords: segment lining; seepage-stress coupling; 3D geological model; TBM water diversion tunnel

Today, almost all rock mass conditions can be bored by modern tunnel boring machines (TBMs) with the tunnel diameter varying from less than 3 m to more than 15 m. The TBMs are among the most technically sophisticated excavation machines in tunnelling industry[1]. The wide application leads to the deep research on the TBM construction technology, and many achievements have been made in construction simulation, structural stability analysis and groundwater pressure calculation. However, in many relevant studies the groundwater pressure was not considered, or was simplified and exerted on the boundary of lining structure[2-4], which is inconsistent with engineering practices and unsafe[5]. The simulation results are more reasonable if the groundwater pressure is exerted as body force, and the seepage-stress coupling calculation can achieve more reliable expression for tunnel stability. The applications of seepage-stress coupling analysis in tunnel engineering are increasingly widespread[6-10], and many achievements have been made. However, most researches were concentrated on solving the settlement and deformation problem. Only a few studies took the groundwater pressure as body force by coupling the seepage field in the stability analysis model to study the groundwater effect. Meanwhile, the tunnel linings in the above studies were treated as impervious materials or homogeneous porous materials due to the limitation of simulation method. Wongsaroj *et al*[11] found there were great differences between the measured pore pressure and numerical simulation results when the shield tunnel lining was treated as uniform permeability. Shin[12] pointed out that the leakage of shield tunnel occurs mainly in partial locations such as segment joints and bolt holes. Therefore, the numerical simulation results will reflect engineering practices better if the leakage of shield tunnel is considered to occur in partial locations. But the relative studies are still rare at present, and

Accepted date: 2014-12-02.
*Supported by the Foundation for Innovation Research Groups of the National Natural Science Foundation of China (No. 51321065), Tianjin Research Program of Application Foundation and Advanced Technology (No. 12JCZDJC29200) and Tianjin Natural Science Foundation (No. 13JCYBJC19500).
Zhong Denghua, born in 1963, male, Dr, Prof.
Correspondence to Zhong Denghua, E-mail: dzhong@tju.edu.cn.

mainly focus on the settlement resulting from partial leakage[13,14].

In summary, the deep-lying TBM water diversion tunnel bears large groundwater pressure and tends to leak in segment joints, but the studies simulating the leakage in segment joints and exerting the groundwater pressure as body force are lack at present. Moreover, the geological models of tunnel engineering are simplified to different extents, and are mostly treated as homogeneous body[2,13,15]. In this paper, a 3D refined geological model of the surrounding rock of a tunnel is established using NURBS-TIN-BReP hybrid data structure[16], and the seepage field considering the leakage in the segment joints of the surrounding rock is simulated based on the geological model. Then, the 3D finite element analysis of TBM water diversion tunnel was carried out coupling the seepage field, obtaining the stress-strain conditions, axial force distributions and bending moment distributions of tunnel lining segment considering the leakage in segment joints.

1 3D geological model

According to the object-oriented classification technique and NURBS-TIN-BRep hybrid data structure, a geological model of the surrounding rock of a tunnel is established in Visual Geo system integrated with multi-source data. The modeling process can be summarized as follows. First of all, based on the object-oriented classification, the modeled objects are categorized according to geometric shapes and attribute characteristics, and the classified geometric models of geological objects and engineering objects are built using NURBS-TIN-BRep hybrid data structure. Then, a 3D integrated model is established by Boolean between 3D geological and engineering objects. Finally, a series of reliability analyses are carried out to ensure the validity and objectivity of the 3D model. Different geological structures are rendered by different colors and textures according to the perturbation function algorithm and the geological drafting standard with actual lithological characteristics and photographs. The 3D refined geological model established above provides an accurate geometric model for seepage analysis and structural analysis. In the meantime, the model has the advantages of small data quantity and high efficiency. The 3D refined geological model of the surrounding rock is shown in Fig. 1.

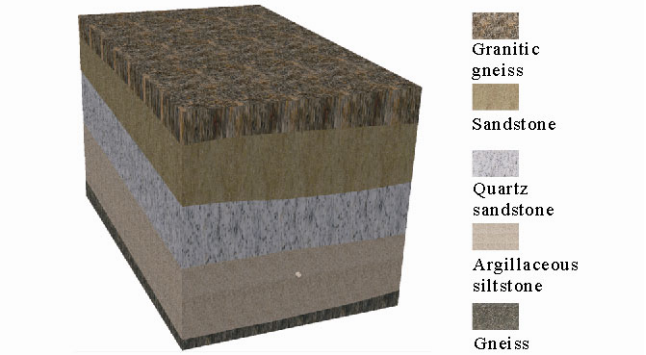

Fig. 1 3D refined geological model of surrounding rock

2 Mathematical model

2.1 Seepage analysis model

The control equations in the seepage analysis consist of the continuity equation and Navier-Stokes equations. The momentum conservation and the viscosity of fluid are taken into consideration in the Navier-Stokes equations.

(1) Continuity equation

$$\frac{\partial \rho}{\partial t}+\frac{\partial(\rho u_i)}{\partial x_i}=0 \tag{1}$$

where t is the time; u_i is the velocity component; x_i is the coordinate component; and ρ is the density.

(2) Navier-Stokes equations

$$\begin{aligned}
&\frac{\partial u}{\partial t}+\operatorname{div}(u\boldsymbol{U})=\operatorname{div}(\upsilon\ \operatorname{grad} u)-\frac{1}{\rho}\frac{\partial p}{\partial x}\\
&\frac{\partial v}{\partial t}+\operatorname{div}(v\boldsymbol{U})=\operatorname{div}(\upsilon\ \operatorname{grad} v)-\frac{1}{\rho}\frac{\partial p}{\partial y}\\
&\frac{\partial w}{\partial t}+\operatorname{div}(w\boldsymbol{U})=\operatorname{div}(\upsilon\ \operatorname{grad} w)-\frac{1}{\rho}\frac{\partial p}{\partial z}
\end{aligned} \tag{2}$$

where $\boldsymbol{U}$ is the velocity vector; u, v, w represent $\boldsymbol{U}$ components in x, y, z directions, respectively; υ is the kinematic viscosity; and p is the pressure on a fluid micro unit.

2.2 Structural analysis model

The proper elastoplastic constitutive model and Mohr-Coulomb yield criterion are used for rock and soil mass. This yield criterion can illustrate different behaviors in tension and compression of geomaterials, and the physical and mechanical parameters are easy to derive through the conventional tests. Moreover, this yield criterion has a better comparability and is widely used in simulating the elastoplastic properties of rock and soil mass. Mathematically, the Mohr-Coulomb yield function can be written as

$$f_s=\sigma_1-\sigma_3\frac{1+\sin\varphi}{1-\sin\varphi}-2c\sqrt{\frac{1+\sin\varphi}{1-\sin\varphi}} \tag{3}$$

where σ_1 and σ_3 are the maximum and minimum principal stress at yield, respectively; c is the cohesion; and φ is the internal friction angle. When $f_s = 0$, it represents the limit equilibrium state of material.

2.3 Coupling of seepage and stress

2.3.1 Seepage body force

As described in seepage mechanics theory, the seepage body force is proportional to the hydraulic gradient. Therefore, the seepage body force in the coordinate directions can be expressed as follows:

$$\begin{Bmatrix} f_x \\ f_y \\ f_z \end{Bmatrix} = \begin{Bmatrix} -\gamma_w \dfrac{\partial H}{\partial x} \\ -\gamma_w \dfrac{\partial H}{\partial y} \\ -\gamma_w \dfrac{\partial H}{\partial z} \end{Bmatrix} = \begin{Bmatrix} \gamma_w J_x \\ \gamma_w J_y \\ \gamma_w J_z \end{Bmatrix} \tag{4}$$

where γ_w is the weight of water; f_x, f_y, f_z are the components of the seepage body force in x, y, z directions, respectively; J_x, J_y, J_z are the components of hydraulic gradient in x, y, z directions, respectively.

2.3.2 Coupling analysis model

The two-step calculation model proposed by Gambolati and Allan[17] is used in this paper, in which the seepage-stress coupling model is composed of seepage analysis model and structural analysis model. The seepage field distributions of the surrounding rock are simulated by the seepage model with the common CFD software STAR-CCM + , while the structural analysis is carried out by the structural model with the software ABAQUS. The meshes used in these two types of software are different. The scripts are developed by the software VisualGeo to solve the data transfer problem between two non-matching meshes[18]. Coupled with the seepage analysis results, the non-uniform distribution of the seepage field is considered in the structural analysis. With the analyses mentioned above, the stress-strain conditions influenced by seepage are comprehensively calculated.

3 Engineering example

A deep-lying water diversion tunnel, with the maximum tunnel axis depth being about 1 028 m and the average tunnel axis depth near 500 m, is located in rock mass rich in groundwater, where the groundwater level is about 100—300 m. The location of the water diversion tunnel is shown in Fig. 2. A TBM with a diameter of 5.95 m was used for excavating in this project. The concrete segment used in this tunnel has an inner diameter of 4.96 m, thickness of 0.28 m and width of 1.6 m. The gap between the segment lining and the surrounding rock is 38 cm at the top arc, and 5 cm at the bottom arc, and will be backfilled by backfilling concrete after fixing segments. The surrounding rock includes 5 strata: granitic gneiss, sandstone, quartz sandstone, argillaceous siltstone, and gneiss. The concrete segment and backfilling concrete are treated as linear elastic materials, while the surrounding rock meets Mohr-Coulomb yield criterion. The mechanical parameters of rock were obtained from the geological investigation report of the project[19], as listed in Tab. 1, in which the permeability coefficient k represents the seepage in the joints of the rock mass.

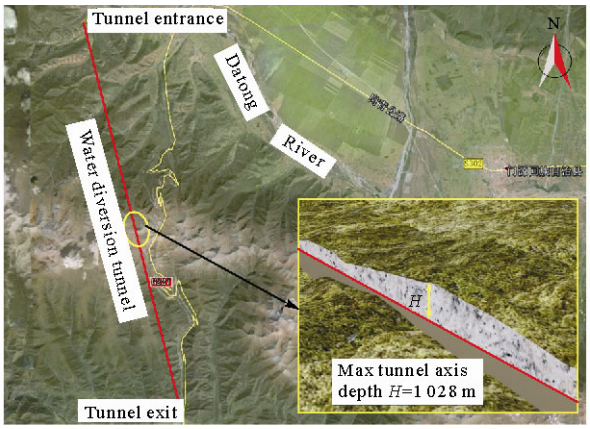

Fig. 2 Water diversion tunnel location

Tab. 1 Mechanical parameters of rocks and structures

Item	ρ/(kg·m^{-3})	E/Pa	μ	k/(m·s^{-1})	φ/(°)	c/MPa
Granitic gneiss	2 580	3.50×10^9	0.26	7.50×10^{-8}	35	1.6
Sandstone	2 500	2.60×10^9	0.33	4.00×10^{-8}	30	0.8
Quartz sandstone	2 550	3.00×10^9	0.30	6.00×10^{-8}	32	1.2
Argillaceous siltstone	2 480	2.10×10^9	0.35	3.50×10^{-8}	25	0.4
Gneiss	2 630	4.00×10^9	0.28	8.00×10^{-8}	40	1.8
Backfilling concrete	2 450	1.70×10^{10}	0.20	1.00×10^{-9}		
Concrete segment	2 500	3.60×10^{10}	0.17			

3.1 Basic hypothesis

(1) The uncertainty of the leakage in segment joints leads to the impossibility of accurately determining the leakage location and quantity. Therefore, the leakage of joints is assumed as uniform.

(2) Different strata are simplified as isotropic continuum material, respectively, and the permeability coefficient is regarded as constant, having no relationship with stress condition.

(3) The steady seepage field after the completion of lining construction is applied to the numerical simulation, and the seepage during tunnel construction period is disregarded.

(4) The segments are tied during simulation since the segments are connected by bolts and will not slide relatively.

3.2 Seepage analysis of surrounding rock

The 3D analysis model of the seepage field is established according to the geo-engineering model of the surrounding rock. The size of the seepage analysis model is about 320 m × 200 m × 200 m (length × width × height). The tunnel axis is located about 150 m away from the top of the model, 100 m away from the sides, and 50 m away from the bottom. In order to realize the simulation of the leakage in segment joints, the TBM segments and segment joints are simplified as faces during modeling, and modeled separately. The segments are regarded as impervious boundary, while the joints are treated as the outlet of the seepage field, and the type of the outlet is the pressure outlet, with the value equal to 0. The element size is about 4 m for the surrounding rock, 0.1 m for backfilling concrete, 5 mm refined for the segment joints. The polyhedral mesh model of the seepage analysis is shown in Fig. 3.

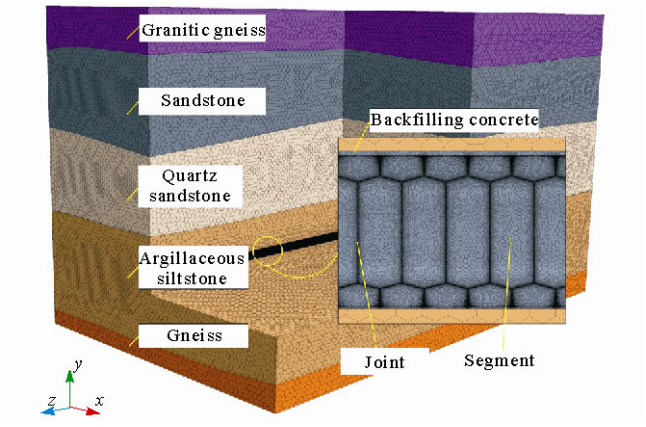

Fig. 3 Polyhedral mesh model of seepage analysis

In the boundary conditions, the upper boundary is the place where the groundwater level is located and the pore pressure is kept constant to be 0 Pa. The lateral boundaries of the model are fixed head boundary, where the pore pressure varies linearly with depth and equals $\rho g(-y)$ Pa. The front-back boundaries of the model are symmetric boundary, and the underside boundary is impermeable boundary.

The hydraulic gradient $J = \Delta p / l$, where l is the seepage path and Δp is the corresponding pressure difference. J_x, J_y, J_z are the components of the hydraulic gradient in x, y, z directions separately, and their values can be extracted from the seepage analysis result. Due to the space limitations, the detailed analysis of the distribution laws of the hydraulic gradient is presented in only one section of this paper, as shown in Fig. 4. The calculation results show that the range of the hydraulic gradient is from 0.000 1 to 0.029 0 for the granitic gneiss stratum, 0.008 6 to 0.059 2 for the sandstone stratum, and 0.031 3 to 0.174 6 for the quartz sandstone stratum. Moreover, the hydraulic gradient within these three strata increases with the depth. The hydraulic gradient of the gneiss stratum varies from 0.001 2 to 0.114, with the maximum hydraulic gradient at the lateral location, and the minimum at the middle region. The argillaceous siltstone stratum, where the tunnel is located, has the maximum hydraulic gradient of 143.0 near the segment joints, i.e., the outlet of the seepage field.

3.3 Structural analysis coupling seepage field

The range affected by tunnel excavation is about 3 times of the tunnel diameter[20]. Therefore, it is suitable for selecting the geological model of the seepage analysis as the geological model of the structural analysis in this paper, according to the general mechanics principle and the feasibility of finite element analysis. The size of the geological model is about 320 m × 200 m × 200 m (length × width × height). The 3D finite element analysis model is established on the basis of the geological model, as shown in Fig. 5.

The method of the coupling seepage analysis can be summarized as follows. Firstly, the hydraulic gradient components J_x, J_y, J_z of all the nodes in the seepage analysis model are extracted from the seepage calculation results. Meanwhile, the centroid coordinates of all the rock mass elements are extracted from the structural analysis model. Secondly, the scripts are developed by the software VisualGeo to solve the data transfer problem between two non-matching meshes, i.e., the model of the

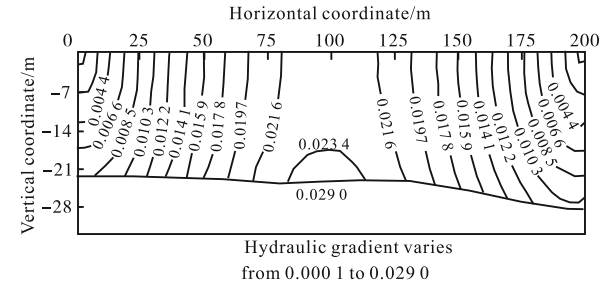

(a) Granitic gneiss

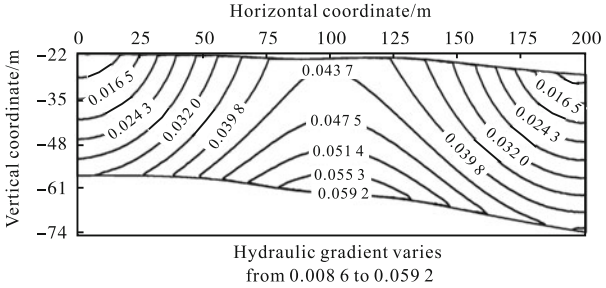

(b) Sandstone

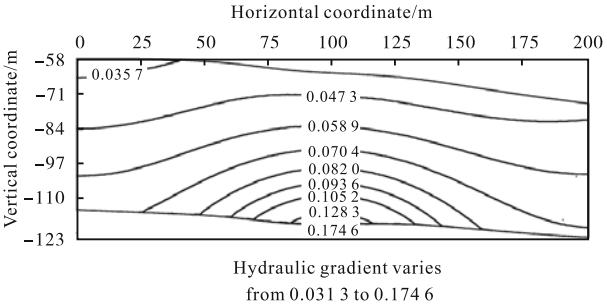

(c) Quartz sandstone

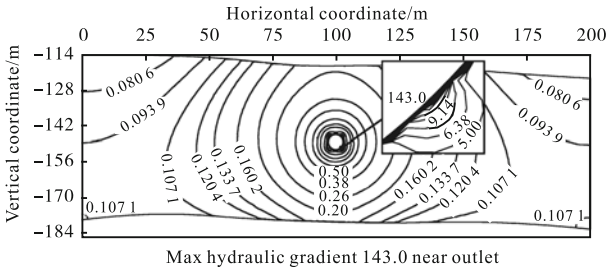

(d) Argillaceous siltstone

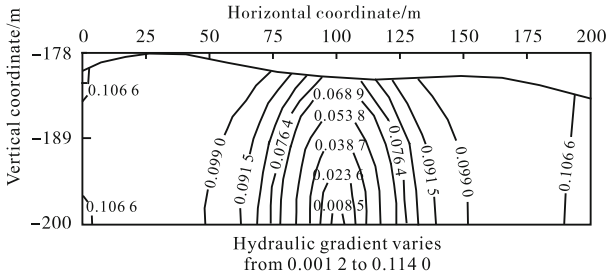

(e) Gneiss

Fig. 4 Distributions of dimensionless hydraulic gradient

seepage simulation and that of the structural analysis simulation. The hydraulic gradient components J_x, J_y, J_z in the three directions of all the rock mass elements in the

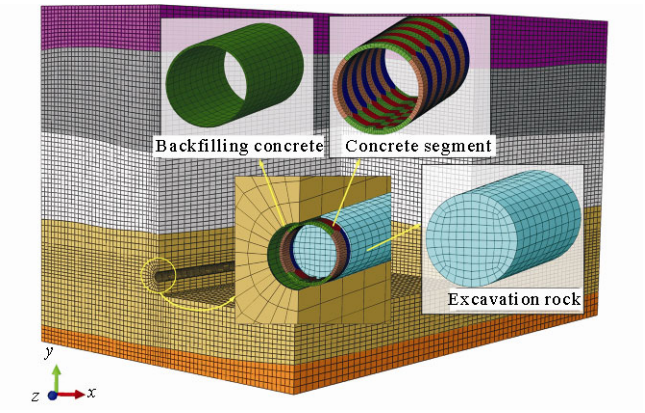

Fig. 5 3D finite element analysis model

structural analysis model are obtained at this step. Then, the seepage body forces in the three directions of all the rock mass elements are derived by using Eq.(4), and coupled into 3D finite element analysis to realize coupling seepage field in the structural analysis model.

The 3D finite element analysis simulation includes the following steps: firstly, the initial stress state is adopted to reach the equilibrium. At this step, it is assumed that this stress varies linearly with the depth and is isotropic, equal to γH. This assumption is reasonable since the coefficient of the horizontal stress for the deep-lying rock approaches 1, indicating a uniform lithostatic stress condition. Secondly, the elastic modulus of excavation rock is reduced to simulate the stress release, and 30% is chosen as the release coefficient by referring to the relevant study[21]. Then, the excavation of the entire tunnel is conducted by removing the excavation rock elements in the tunnel geometry. Subsequently, the backfilling concrete elements and concrete segment elements are activated to simulate the completion of the lining construction. At this step, the segment stress-strain condition and the distributions of the axial force as well as the bending moment under the condition of disregarding the groundwater pressure can be obtained. Finally, the seepage field is coupled into the structural analysis to simulate the segment stress-strain condition and the distributions of the axial force as well as the bending moment considering the leakage in the segment joints.

3.3.1 Segment deformation

The nephograms of the segment radical displacement under the conditions of disregarding the groundwater pressure and coupling the seepage field are shown in Fig. 6, respectively. According to the calculation results, the distributions of the segment radial displacement under these two conditions are different. The maximum radial displacement under the condition of disregarding

the groundwater pressure and the condition of coupling the seepage field is 1.932 mm and 3.108 mm respectively, which occurs at the bottom segment and top segment respectively. The positive values in Fig. 6 represent the deformation deviating from the circular center, while the negative values represent the deformation pointing to the circular center. It can be known from Fig. 6 that the deformation of the side segment deviates from the circular center, and is relatively small, but it is relatively large and toward the circular center for the top and bottom segments. When comparing the radial displacement distributions under these two conditions, it is easy to find out that the groundwater pressure changes the distributions of the radial displacement, changing the maximum deformation location from the bottom to the top, and increasing the maximum radial displacement from 1.932 mm to 3.108 mm, which will lead to the increase of risk and decrease of security.

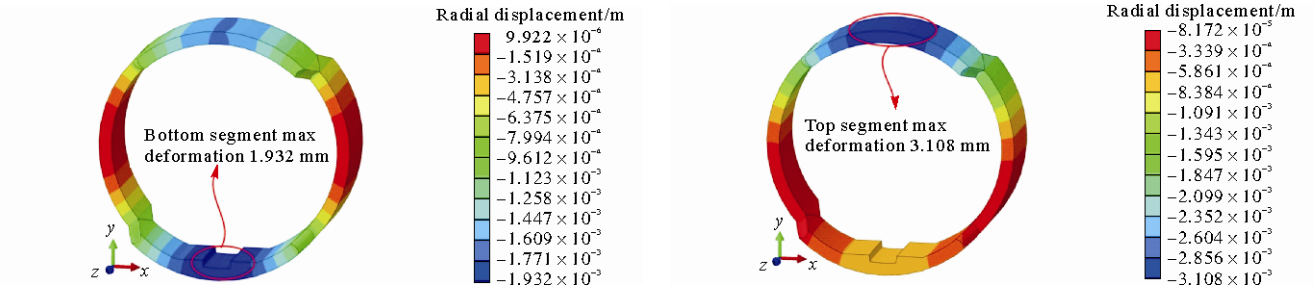

(a) Disregarding groundwater pressure (b) Coupling seepage field

Fig. 6 Nephogram of radial displacement

3.3.2 Segment stress distribution

The distributions of the minimum principal stress σ_3 and the maximum principal stress σ_1 under the two conditions are shown in Fig. 7. The calculation results show that the stress distributions under the two conditions are basically similar, the minimum principal stress σ_3 is distributed inside the side segment, as shown in Fig. 7(a) and Fig. 7(c), and the maximum principal stress σ_1 is distributed in the partial area outside the bottom segment, as shown in Fig. 7(b) and Fig. 7(d). Under the condition of disregarding the groundwater pressure, the range of the principal stress varies from – 17.64 MPa to 1.12 MPa. As for the condition of coupling the seepage field, the corresponding range is from – 21.31 MPa to 1.35 MPa. The axial compressive and tensile strength limitations of the lining segment concrete are 23.1 MPa and 1.89 MPa, respectively. The principal stress is within the allowable range, therefore, the stability of tunnel lining segment meets the requirement. The minimum principal stress and the maximum principal stress under the condition of coupling the seepage field are larger compared with the condition of disregarding the groundwater pressure. It is obvious that the groundwater pressure makes the maximum and minimum principal stress increase by 20.80% and 20.54%, respectively, which may cause the instability of the tunnel. Thus it is of great importance to take the groundwater pressure into consideration during the tunnel design and construction.

The leakage occurring in the segment joints is taken into consideration in this paper, obtaining the seepage field of the surrounding rock, which is closer to engineering practices. Due to the small permeability coefficients of the surrounding rock and backfilling concrete, only small partial areas of the seepage field in the surrounding rock near the segment joints are affected, as shown in Fig. 4(d). Meanwhile, the concrete stiffness of the lining segments is relatively large. Therefore, there are no larger stress and deformation near the segment joints for the lining segments, as shown in Fig. 6 and Fig. 7.

3.3.3 Axial force and bending moment

A stress path was set along the segment thickness in each angle of the segment, and the stress distributions were extracted along the stress path. Then the distributions of the axial force and bending moment were obtained by integration along the stress path. The axial force distributions of the segment are shown in Fig. 8. In this figure, $\theta = 0°$ and $\theta = 180°$ indicate the top and the bottom of the segment, respectively. The positive value represents the compressive force while the negative value means the tensile force. It can be seen from Fig. 8 that the segment is compressed in every angle of the circle under the two conditions, and the axial forces under the condition of coupling the seepage field are larger than the corresponding values under the condition of disregarding the groundwater pressure in every angle. The maximum axial forces under the two conditions are all located at $\theta = 90°$. The value under the condition of disregarding the groundwater pressure is 4 413 kN, while the correspond-

ing value is 5 449 kN under the condition of coupling the seepage field, meaning that the maximum axial force increased by 23.5% under the effect of the groundwater pressure.

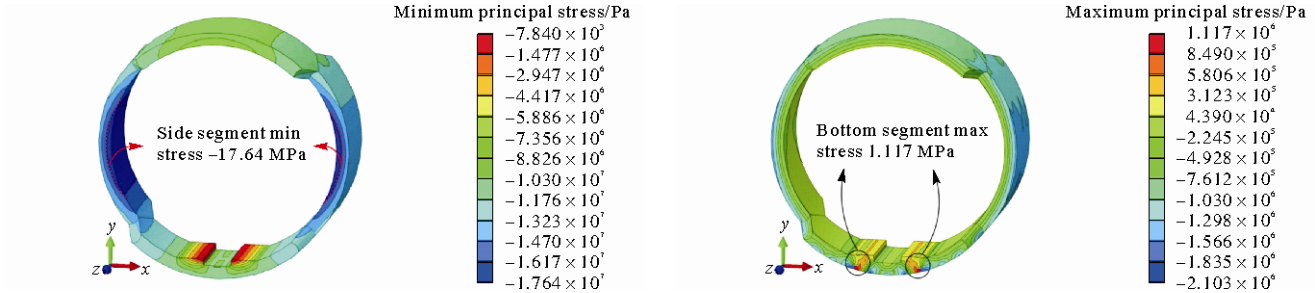

(a) σ_3 when disregarding groundwater pressure

(b) σ_1 when disregarding groundwater pressure

(c) σ_3 when coupling seepage field

(d) σ_1 when coupling seepage field

Fig. 7 Nephogram of the maximum and minimum principal stress

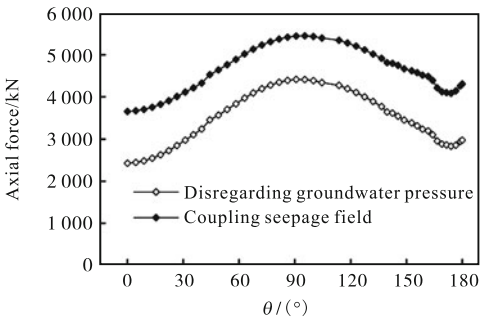

Fig. 8 Axial force distributions of segment

The bending moment distributions of the segment are shown in Fig. 9. The bending moment results from the non-uniform distributions of the stress along the segment thickness. It can be deduced from Fig. 9 that the non-uniformity of the stress distributions along the segment thickness at the side segment under the two conditions are almost the same because of the same bending moment distributions. But they are different for the top and bottom segments, and the non-uniform degree under the condition of disregarding the groundwater pressure is more obvious because of the larger bending moment. The maximum bending moment under the condition of disregarding the groundwater pressure is 99.23 kN·m, and the value under the other condition is 82.68 kN·m. The extreme values of bending moment distributions are located near the areas where $\theta = 0°$, 90°, 180°. Thus, it is recommended to take some reinforcement measures in these areas in the actual design and construction to ensure the safe operation of the tunnel.

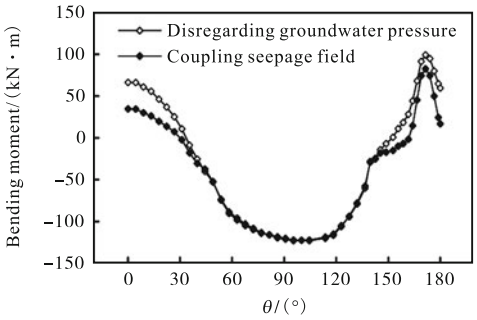

Fig. 9 Bending moment distributions of segment

4 Conclusions

(1) A 3D refined geological model has been established using NURBS-TIN-BReP hybrid data structure, providing a geological model reflecting real geological conditions for the numerical simulation.

(2) The models of the segments and joints have been established separately based on the 3D refined geo-

logical model, in which the segments are impervious boundary, while the joints are the outlet of the seepage field, and the seepage field of the surrounding rock is simulated considering the leakage occurring in the segment joints.

(3) The scripts are developed by the software VisualGeo to solve the data transfer problem between the seepage field and stress field, and the groundwater pressure considering the leakage in the segment joints is coupled with the structural analysis model as body force.

References

[1] Zhao K, Janutolo M, Barla G. A completely 3D model for the simulation of mechanized tunnel excavation[J]. *Rock Mechanics and Rock Engineering*, 2012, 45(4): 475-497.

[2] Zhao Wuxin, He Xianzhi, Chen Weizhong *et al*. Method for analyzing seismic response of shield tunnel and its application[J]. *Rock and Soil Mechanics*, 2012, 33(8): 2415-2421(in Chinese).

[3] Wang Fei, Miao Linchang, Li Chunlin. Numerical analysis of shield tunnel settlement considering construction process[J]. *Chinese Journal of Rock Mechanics and Engineering*, 2013, 32(Suppl 1): 2907-2914(in Chinese).

[4] Yao Chaofan, Yan Qixiang, He Chuan *et al*. An improved analysis model for shield tunnel with double-layer lining and its applications[J]. *Chinese Journal of Rock Mechanics and Engineering*, 2014, 33(1): 80-89(in Chinese).

[5] Wang Jianxiu, Yang Lizhong, He Jing. Introduction to the calculation of external water pressure of tunnel lining[J]. *Chinese Journal of Rock Mechanics and Engineering*, 2002, 21(9): 1339-1343(in Chinese).

[6] Liu Zhongqiu, Zhang Qing. Damage evolution analysis of permeable lining of deep diversion tunnel based on seepage-stress coupling theory[J]. *Chinese Journal of Rock Mechanics and Engineering*, 2012, 31(10): 2147-2153(in Chinese).

[7] Xu Jinhua, He Chuan, Xia Weiyang. Research on coupling seepage field and stress field analysis of underwater shield tunnel[J]. *Rock and Soil Mechanics*, 2009, 30(11): 3519-3527(in Chinese).

[8] Thomas Kasper, Gunther Meschke. A 3D finite element simulation model for TBM tunnelling in soft ground[J]. *International Journal for Numerical and Analytical Methods in Geomechanics*, 2004, 28(14): 1441-1460.

[9] Zhang Yitong, Zhu Long, Ning Jiaxing. Analysis on stability of shield tunnelling face in soil with strain-softening behavior[J]. *Journal of Tianjin University*: *Science and Technology*, 2013, 46(7): 596-602(in Chinese).

[10] Arjnoi P, Jeong Jae-Hyeung, Kim Chang-Yong *et al*. Effect of drainage conditions on porewater pressure distributions and lining stresses in drained tunnels[J]. *Tunnelling and Underground Space Technology*, 2009, 24(6): 376-389.

[11] Wongsaroj J, Soga K, Mair R J. Modeling of long-term ground response to tunnelling under St James's Park, London[J]. *Geotechnique*, 2007, 57(1): 75-90.

[12] Shin J H. A numerical study of the effect of groundwater movement on long-term tunnel behaviour[J]. *Geotechnique*, 2002, 52(6): 391-403.

[13] Wu Huaina, Hu Mengda, XuYeshuang *et al*. Law of influence of segment on long-term tunnel settlement[J]. *Chinese Journal of Underground Space and Engineering*, 2009, 5(Suppl 2): 1608-1611(in Chinese).

[14] Liu Yin, Zhang Dongmei, Huang Hongwei. Influence of long-term partial drainage of shield tunnel on tunnel deformation and surface settlement[J]. *Rock and Soil Mechanics*, 2013, 34(1): 290-299(in Chinese).

[15] Rohola Hasanpour, Jamal Rostami, Bahtiyar Ünver. 3D finite difference model for simulation of double shield TBM tunnelling in squeezing grounds[J]. *Tunnelling and Underground Space Technology*, 2014, 40: 109-126.

[16] Zhong Denghua, Li Mingchao, Liu Jie. 3D integrated modeling approach to geo-engineering objects of hydraulic and hydroelectric projects[J]. *Science in China Series E*: *Technological Sciences*, 2007, 50(3): 329-342.

[17] Gambolati G, Allan F R. Mathematical simulation of the subsidence of Venice[J]. *Water Resour Res*, 1973, 9: 721-733.

[18] Zhong Denghua, Zhang Xiaoxin, Ao Xuefei *et al*. Study on coupled 3D seepage and stress fields of the complex channel project[J]. *Science China - Technological Sciences*, 2013, 56(8): 1906-1914.

[19] Changjiang Institute of Survey, Planning, Design and Research. The Geological Investigation Report of Yindajihuang Water Diversion Engineering in Qinghai Province[R]. Changjiang Institute of Survey, Planning, Design and Research, Wuhan, China, 2010(in Chinese).

[20] Zhong Denghua, Tong Dawei. 3D finite element simulation of tunnel boring machine construction processes in deep water conveyance tunnel[J]. *Transactions of Tianjin University*, 2009, 15(2): 101-107.

[21] Yang Linde, Ding Wenqi. A study on the design of permeable R. C. lining in high pressure water carriage tunnel[J]. *Chinese Journal of Rock Mechanics and Engineering*, 1997, 16(2): 112-117(in Chinese).

(Editor: Liu Wenge)